Coarsening in potential and nonpotential models of oblique stripe patterns

J. R. Gomez-Solano and D. Boyer*

Instituto de Física, Universidad Nacional Autónoma de México, Apartado Postal 20-364, 01000 México, Distrito Federal, Mexico
(Received 16 May 2007; published 24 October 2007)

We study the coarsening of two-dimensional oblique stripe patterns by numerically solving potential and nonpotential anisotropic Swift-Hohenberg equations. Close to onset, all models exhibit isotropic coarsening with a single characteristic length scale growing in time as $t^{1/2}$. Further from onset, the characteristic lengths along the preferred directions $\hat{x}$ and $\hat{y}$ grow with different exponents, close to 1/3 and 1/2, respectively. In this regime, one-dimensional dynamical scaling relations hold. We draw an analogy between this problem and model A in a stationary, modulated external field. For deep quenches, nonpotential effects produce a complicated dislocation dynamics that can lead to either arrested or faster-than-power-law growth, depending on the model considered. In the arrested case, small isolated domains shrink down to a finite size and fail to disappear. A comparison with available experimental results for electroconvection in nematics is presented.

I. INTRODUCTION

Domain coarsening of uniform phases in systems locally in thermal equilibrium has received a lot of attention over the past decades [1,2]. After quenching a system below a transition point, ordered regions of the lower symmetry phase form, and their characteristic length L grows slowly, usually as a power law at large times, $L \sim t^n$. A number of theoretical schemes based on the dynamical scaling hypothesis and on the study of the relaxation of topological defects have been proposed to infer coarsening exponents and address their universality [2–7].

Less understood is the phase ordering kinetics in systems driven out of equilibrium, in particular those forming dissipative structures like regular patterns. The basic nonequilibrium structures are the modulated phases (stripes) of well-defined periodicity that appear above an instability threshold in thermal convection of fluids, in driven chemical reactors, or in electroconvection of nematic liquid crystals [8–11].

A body of numerical results [12–25] suggests that the ordering kinetics of stripe patterns following a quench is not universal but model dependent, and even parameter dependent. Modulated phases in isotropic systems actually exhibit a rich variety of topological defects (dislocations, disclinations, grain boundaries) not observed in uniform phases. There might exist many mechanisms controlling the coarsening of stripe patterns: for instance, the annihilation of disclination quadrupoles, as observed experimentally [26–28] in block-copolymer melts with cylindrical mesophases (leading to $n=1/4$), or grain boundary motion in the Swift-Hohenberg model close to onset ($n=1/3$) [17,19,20,24].

For a given system, the growing length scale may even be nonunique and the dynamical scaling hypothesis not satisfied. Different defect-based definitions of the size L of the ordered striped domains can lead to different coarsening exponents [14,16,21,22]. This effect seems to be more pronounced far from the onset of stripe formation. In this regime, the growth of order often becomes very slow or

arrested [15], in particular due to pattern-induced pinning effects acting on defects [17,19,24].

In addition, unlike equilibrium phases, the dynamics of nonequilibrium patterns is *a priori* not driven by the minimization of a free-energy functional but better modeled by nonpotential (nonrelaxational) equations [8,10,11,29]. Recent simulations of the Boussinesq equations for Rayleigh-Bénard convection [22] suggest that multiple length scales must be defined to characterize the coarsening of nonpotential stripe patterns. Adding nonpotential terms to potential models [14,30] (or, similarly, taking into account hydrodynamics in the order parameter description of block-copolymer melts [25]) can noticeably increase some coarsening rates and lead to qualitative changes in the structure of the defected patterns.

In this context, systems forming anisotropic patterns have recently attracted particular attention [31–35]. An example are the oblique phases, composed of stripes that make a fixed angle θ or $-\theta$ with respect to some $\hat{x}$ axis. Domain coarsening in these systems has been studied in detail experimentally in electroconvection of nematics [31–33]. Anisotropic stripes may be regarded as topologically simpler than isotropic ones because of their finite number of orientations. However, some challenging difficulties mentioned above for isotropic systems still remain, such as the presence of various sorts of defects and nonpotential effects.

The experimental studies of Refs. [31,32] on oblique stripes report that chevron grain boundaries and dislocation arrays (the domain interfaces along the $\hat{x}$ and $\hat{y}$ directions, respectively) have very different mobilities. After a quench, their respective densities have different power-law decays with time, both with unusually small exponents. These results remain largely unexplained theoretically. A first numerical study [34] based on a potential anisotropic Swift-Hohenberg equation for oblique stripes [36] reproduced the decay of the dislocation density but predicted a much faster ordering in the y direction than observed experimentally.

We reconsider this problem by introducing in Sec. II nonpotential versions (never considered before, to our knowledge) of the anisotropic model used in [34]. The wave numbers selected in these models are comparable to the

*boyer@fisica.unam.mx

experimental ones. In Sec. III, we define an orientational order parameter, its correlation lengths along the preferred $\hat{x}$ and $\hat{y}$ directions, and the defect densities (chevron and dislocations). In Sec. IV, we find two robust coarsening regimes at moderate quench depths, independent of the potential or nonpotential nature of the models: an isotropic regime very close to onset and an anisotropic one (in partial agreement with experiments) at intermediate quenches. One-dimensional dynamical scaling relations hold in the latter case. In Sec. V, we show that, up to moderate quenches, the problem can be approximately reduced to model A [3] in a stationary, spatially modulated external field. Far from onset, nonpotential effects can lead to arrested or very fast domain growth, depending on the model. In the arrested case, small domains shrink down only to a finite size. Conclusions are presented in Sec. VI.

II. BASIC MODELS AND THEIR FIRST-ORDER AMPLITUDE EQUATIONS

An electroconvection setup consists of a doped nematic liquid crystal confined between two plates with planar alignment. When an ac transverse electric field is applied, normal or oblique stripes (among other patterns) can form depending on the frequency [37–40]. Some time ago, Pesch and Kramer (PK) introduced a phenomenological Swift-Hohenberg-like model that exhibits a transition from normal to oblique rolls [36]:

$$\partial_t \psi = r\psi - \zeta^4(\nabla^2 + k_0^2)^2\psi - \frac{c}{k_0^4}\partial_y^4\psi + \frac{2\eta}{k_0^4}\partial_x^2\partial_y^2\psi + \mathcal{N}[\psi],$$
(1)

where $\psi(\vec{r},t)$ is the local order parameter, $\mathcal{N}[\psi]=-\psi^3$, c and η are dimensionless anisotropy parameters, k_0 is a characteristic wave number, ζ (set to $1/k_0$ in the following) is the coherence length, and r is the main control parameter. In electroconvection of nematics with planar alignment, x is the coordinate in the direction parallel to the undistorted director.

Linear stability analysis of the uniform state $\psi(\vec{r},t)=0$ of Eq. (1) against small periodic perturbations $\delta\psi(\vec{r},t) = \delta\psi_0 \exp(i\vec{k}\cdot\vec{r}+\sigma t)$ gives the dispersion relation

$$\sigma(p,q) = r - \frac{1}{k_0^4}[\zeta^4 k_0^4(k_0^2 - p^2 - q^2)^2 + cq^4 - 2\eta p^2 q^2], \quad (2)$$

where $\vec{k}=p\hat{x}+q\hat{y}$. Maximizing (2) with respect to p and q and looking for the values of r for which $\sigma=0$, one finds that some modes of finite wave number become marginally unstable when the control parameter r exceeds the critical value $r_c^{(n)}$ or $r_c^{(o)}$:

$$r_c^{(n)} = 0, \quad \{p_c^2 = k_0^2, \; q_c^2 = 0\}, \quad \text{normal stripes}, \quad (3)$$

$$r_c^{(o)} = \frac{-\eta^2}{c+2\eta-\eta^2} < 0, \quad \begin{cases} p_c^2 = \frac{c+\eta}{c+2\eta-\eta^2}k_0^2, \\ \\ q_c^2 = \frac{\eta}{c+2\eta-\eta^2}k_0^2 \end{cases}, \quad \text{oblique stripes}, \quad (4)$$

where we have assumed that $c > 0$. The marginally unstable wave vectors in the oblique case make an angle θ or $-\theta$, with respect to the x axis, where $\theta=\arctan[\sqrt{\eta/(c+\eta)}]$. These two degenerate oblique modes, denoted as $\vec{k}_c^+$ (zig) and $\vec{k}_c^-$ (zag) in the following, are observed for $\eta > 0$ only. The model Eq. (1) actually reproduces the transition from normal to oblique stripes when η is tuned from negative to positive values.

In the following, we define the reduced control parameter as

$$\varepsilon = r - r_c^{(o)}. \quad (5)$$

Numerical solutions of Eq. (1) with random initial conditions for the field ψ lead to the formation of oblique stripes if $c > 0$, $\eta > 0$, and $r > 0$ (i.e., $\varepsilon > |r_c^{(0)}|$). Normal stripes were never observed close to onset for the parameter values used in this study.

Domain coarsening in anisotropic oblique stripe patterns was recently studied with Eq. (1) [34]. This model has a potential structure, as it can be written as $\partial_t\psi=-\delta F/\delta\psi$, with F a Lyapunov functional given by

$$F = \frac{1}{2k_0^4}\int d\vec{r}\{k_0^4(-r\psi^2 + \psi^4/2) + k_0^4\zeta^4[(k_0^2 + \nabla^2)\psi]^2 - 2\eta(\partial_x\partial_y\psi)^2 + c(\partial_y^2\psi)^2\}.$$
(6)

We propose here two nonrelaxational extensions of (1) by replacing the $-\psi^3$ nonlinearity by terms that do not derive from a functional. We consider the cases

$$\mathcal{N}[\psi] = -\psi^3 - \frac{c_1}{k_0^2}\psi(\nabla\psi)^2 + \frac{c_2}{k_0^2}\psi^2\nabla^2\psi, \quad \text{model I}, \quad (7)$$

$$\mathcal{N}[\psi] = \frac{c_3}{k_0^4}\nabla^2\psi(\nabla\psi)^2 + \frac{3-c_3}{k_0^2}(\partial_i\psi)(\partial_j\psi)(\partial_i\partial_j\psi), \quad \text{model II}, \quad (8)$$

where c_1, c_2, c_3 are constants and $(i,j)=(x,y)$. These terms were previously considered in the isotropic Swift-Hohenberg model of Rayleigh-Bénard convection [41] (see also [14]). Expressions (7) and (8) are nonpotential when $c_1 \neq -c_2$ and $c_3 \neq 2$. We set $c_1=c_2=1$ and $c_3=3$ in the following.

As shown in the next section, all the above models with random initial conditions lead to the formation of polycrystalline configurations like the one shown in Fig. 1. Their large time evolution is controlled by the motion of grain boundaries separating domains of perfectly oriented zig and zag stripes. To describe patterns containing grain boundaries, we look for general solutions of the model equations of the form [29,42]

$$\psi(\vec{r},t) = A^+(\vec{r},t)e^{i\vec{k}_c^+\cdot\vec{r}} + A^-(\vec{r},t)e^{i\vec{k}_c^-\cdot\vec{r}} + \text{c.c.}, \quad (9)$$

where $\vec{k}_c^\pm=p_c\hat{x}\pm q_c\hat{y}$, with p_c and q_c positive and given by Eq. (4); c.c. means the complex conjugate. Solutions of the form (9) describe polycrystalline states of zig and zag domains with wave vectors close to the marginal ones. $A^+ \neq 0$ and $A^- \simeq 0$ within a zig domain, and vice versa. The amplitudes A^+ and A^- are both nonvanishing in the vicinity of a grain boundary.
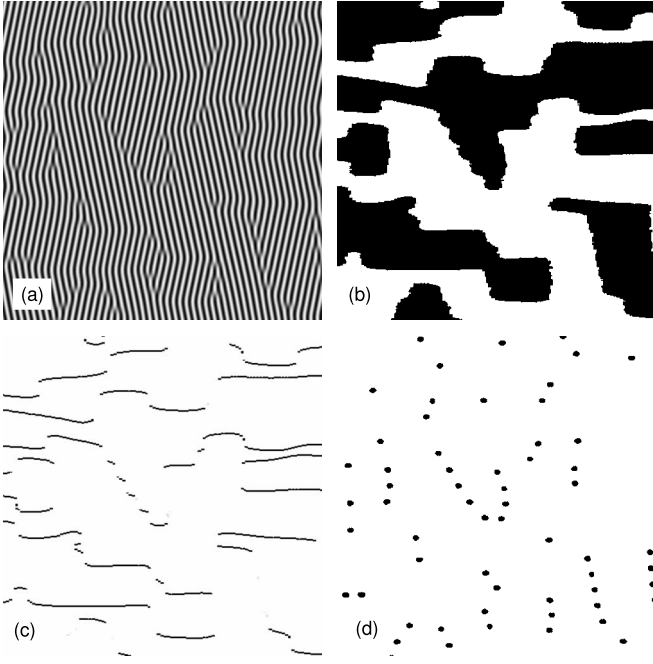
FIG. 1. (a) Oblique stripe pattern at $t=500$ obtained by numerically solving Eq. (7) (model I) with $\varepsilon=0.4118$, $c=12$, $\eta=0.5$, and $c_1=c_2=1$; (b) domain configuration of the stripe pattern in (a); (c) chevron boundaries of (a); (d) dislocations of (a). We show a fraction of 400×400 nodes from a total discretized system of size 1024×1024.

In the limit $\varepsilon\ll1$, the multiple-scale formalism [29,36] can be applied to the three models (1), (7), and (8). We find that, at first order in $\varepsilon^{1/2}$, the dynamics of A^+ and A^- is described by two coupled Ginzburg-Landau equations

$$\partial_t A^+ = \varepsilon A^+ + \frac{4}{k_0^4}[p_c^2\partial_x^2 + 2(1-\eta)p_cq_c\partial_x\partial_y + (1+c)q_c^2\partial_y^2]A^+$$
$$- 3\gamma|A^+|^2A^+ - 6\gamma|A^-|^2A^+, \tag{10}$$

$$\partial_t A^- = \varepsilon A^- + \frac{4}{k_0^4}[p_c^2\partial_x^2 - 2(1-\eta)p_cq_c\partial_x\partial_y + (1+c)q_c^2\partial_y^2]A^-$$
$$- 3\gamma|A^-|^2A^- - 6\gamma|A^+|^2A^-, \tag{11}$$

where γ is a constant parameter whose expression depends on the model considered,

$$\gamma = \begin{cases} 1, & \text{potential PK model,} \\ 1 + \dfrac{c_1+3c_2}{3}\left(\dfrac{c+2\eta}{c+2\eta-\eta^2}\right), & \text{model I,} \\ \left(\dfrac{c+2\eta}{c+2\eta-\eta^2}\right)^2, & \text{model II.} \end{cases}$$

Equations similar to (10) and (11) were proposed as reduced models of oblique patterns in electroconvection [43,44] and thermoconvection [45] of nematics with planar alignment close to onset. They can be recast as $\partial_t A^+ = -\delta F_{GL}/\delta\bar{A}^+$ and $\partial_t A^- = -\delta F_{GL}/\delta\bar{A}^-$, where F_{GL} is a Lyapunov functional given by

$$F_{GL} = \int d\vec{r}\left(-\varepsilon(|A^+|^2 + |A^-|^2) + \frac{4}{k_0^4}|[p_c\partial_x + (1-\eta)q_c\partial_y]A^+|^2\right.$$

$$+ \frac{4}{k_0^4}|[p_c\partial_x - (1-\eta)q_c\partial_y]A^-|^2 + \frac{4\eta}{k_0^2}(|\partial_y A^+|^2 + |\partial_y A^-|^2)$$

$$\left. + \frac{3}{2}\gamma(|A^+|^4 + |A^-|^4) + 6\gamma|A^+|^2|A^-|^2\right), \tag{12}$$

where $\bar{A}$ is the complex conjugate of A. Close to onset ($\varepsilon\ll1$), the amplitude equations of anisotropic oblique striped domains are identical for the three models (1), (7), and (8) up to the multiplicative constant γ (which can be absorbed in the amplitude, time, and space scales). The amplitude equations have a potential structure even when deriving from a nonpotential model. We therefore expect that very close to onset oblique stripe patterns exhibit a generic ordering dynamics, independently of the potential or nonpotential nature of the system. The amplitude Eqs. (10) and (11) will be used to discuss some aspects of the coarsening process close to onset in Sec. V A. For a more detailed description of defect dynamics far from onset, higher order contributions $[O(\varepsilon^2)]$ would be needed in the derivation of the amplitude and phase equations [8,29].

III. NUMERICAL METHOD

Equation (1) with the nonlinear term (7) or (8) is numerically solved by using a semi-implicit pseudospectral method and a time integration procedure described in [46]. The two-dimensional space is discretized on a square grid of mesh size $\Delta x=1$ with 1024×1024 nodes. The characteristic wavelength is set to $\lambda_0=2\pi/k_0=8\,\Delta x$. The time integration scheme is stable for large values of the time step Δt. We set $\Delta t=0.5$ for all the values of the quench depth studied. The initial condition for ψ is a random field with Gaussian distribution, of mean $\langle\psi\rangle=0$ and variance $\langle\psi^2\rangle=\varepsilon$. Numerical results are averaged over ten different initial conditions for each model and value of ε.

Given relation (5) and the fact that a random initial Gaussian field will evolve toward oblique patterns only if $r>0$, we choose the parameters in Eq. (1) such that the smallest possible quench ($\varepsilon_{min}=-r_c^{(o)}$) is small compared with unity. We set $c=12$ and $\eta=0.5$ in all the calculations, corresponding to $-r_c^{(o)}=0.0196$ and $\theta=11.31°$ ($\vec{k}_c^\pm/k_0 = 0.9901\hat{x}\pm0.1980\hat{y}$).

A typical configuration of oblique stripe domains is displayed in Fig. 1(a) at $t=500$ in the case of model I for a moderate quench. As observed in electroconvection experiments [31,32] and previous numerical simulations of (1) [34], interfaces separating zig and zag stripes are mainly of two kinds: horizontal chevron boundaries where stripes change their orientation from θ to $-\theta$ without any phase singularity, and slightly curved boundaries composed of arrays of dislocations with an orientation close to the vertical direction. Close to onset, isolated dislocations are scarcely observed within domains and do not seem to control the ordering dynamics. Note that isolated dislocations in anisotropic patterns are analogous to superfluid vortices, which

are known to have a diverging energy [47]. This is due to the fact that, unlike those of isotropic stripes, the spatial derivatives in the first-order amplitude Eqs. (10) and (11) can be recast into a Laplacian form after an axis rotation.

Zig and zag domains can be identified by means of a (scalar) orientational local order parameter ψ_d, defined as

$$\psi_d(\vec{r},t) = \begin{cases} +1 & \text{if } (\partial_x\psi)(\partial_y\psi) \geq 0 \quad \text{(zig)}, \\ -1 & \text{if } (\partial_x\psi)(\partial_y\psi) < 0 \quad \text{(zag)}. \end{cases}$$

The orientation field ψ_d of the pattern of Fig. 1(a) is shown in Fig. 1(b).

Due to the anisotropy of the problem, we measure the growth of order along the $\hat{x}$ and $\hat{y}$ directions separately. For this purpose we introduce an orientational structure factor, defined as

$$S(\vec{q},t) \equiv \langle \widetilde{\psi}_d(\vec{q},t)\widetilde{\psi}_d(-\vec{q},t) \rangle, \tag{13}$$

where $\widetilde{\psi}_d$ is the two-dimensional (2D) Fourier transform of ψ_d and the angular brackets indicate averages over different initial conditions. We define the one-dimensional structure factors along $\hat{x}$ and $\hat{y}$ as

$$S_x(q_x,t) = \int_{-\infty}^{+\infty} S(\vec{q},t)dq_y \tag{14}$$

and

$$S_y(q_y,t) = \int_{-\infty}^{+\infty} S(\vec{q},t)dq_x, \tag{15}$$

respectively. It can easily be shown that (14) and (15) are the 1D Fourier transforms of the equal time correlation functions along the directions $\hat{x}$ and $\hat{y}$, respectively,

$$C_x(x,t) = \int \langle \psi_d(\vec{r}',t)\psi_d(\vec{r}' + x\hat{x},t) \rangle d\vec{r}', \tag{16}$$

$$C_y(y,t) = \int \langle \psi_d(\vec{r}',t)\psi_d(\vec{r}' + y\hat{y},t) \rangle d\vec{r}'. \tag{17}$$

We define the correlation lengths in the $\hat{x}$ and $\hat{y}$ directions from the inverse width of the curves $S_x(q_x,t)$ and $S_y(q_y,t)$ in Fourier space:

$$L_x(t) = \left(\frac{\int_{-\infty}^{\infty} |q_x|S_x(q_x,t)dq_x}{\int_{-\infty}^{\infty} S_x(q_x,t)dq_x} \right)^{-1}, \tag{18}$$

$$L_y(t) = \left(\frac{\int_{-\infty}^{\infty} |q_y|S_y(q_y,t)dq_y}{\int_{-\infty}^{\infty} S_y(q_y,t)dq_y} \right)^{-1}. \tag{19}$$

As in isotropic systems, the defect densities should be related to the correlation lengths defined above if dynamical scaling holds. In the case of oblique stripe domains, we investigate
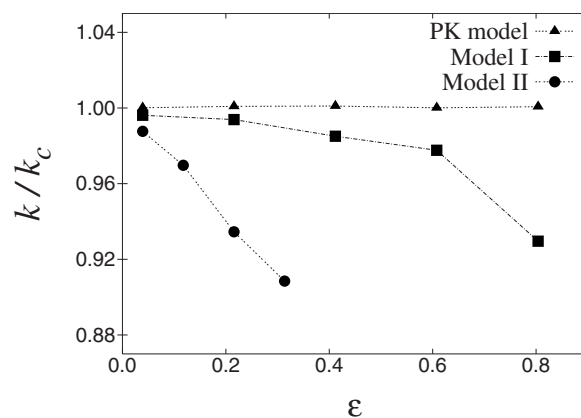

FIG. 2. Selected wave number as a function of ε for the three models studied.

separately the evolution of chevron (ρ_{ch}) and dislocation (ρ_{dis}) densities. Chevron boundaries are identified as the lattice nodes (x',y') where

$$|\psi_d(x',y'+1,t) - \psi_d(x',y',t)| = 2. \tag{20}$$

The chevron density is defined as the fraction of such nodes, marked in black in Fig. 1(c). We do not consider as belonging to a chevron boundary isolated horizontal clusters of nodes satisfying (20) that are shorter than half the stripe period. Dislocations are identified by using the filtering procedure described in [15]. A typical configuration of dislocations is shown in Fig. 1(d), corresponding to the pattern of Fig. 1(a). We define numerically ρ_{dis} as the fraction of area occupied by the black regions in Fig. 1(d).

IV. RESULTS

A. Wave number selection

Before investigating domain growth, we address the issue of wave number selection at short times, as it can play an important role in the subsequent defect dynamics [14,22,30,40]. The wave number k of the background stripes at time t is numerically obtained by averaging the modulus of the four wave vectors where the order parameter structure factor $\langle \widetilde{\psi}(\vec{q},t)\widetilde{\psi}(-\vec{q},t) \rangle$ is maximum ($\widetilde{\psi}$ being the Fourier transform of ψ).

As for isotropic potential equations [8,9], the selected wave number k in the PK model (1) is the one that minimizes the Lyapunov functional (6). After a short transient k reaches an asymptotic value that is independent of ε, as shown in Fig. 2, and given by the marginal wave number maximizing the growth rate (2),

$$k_c = \sqrt{p_c^2 + q_c^2} = \sqrt{\frac{c+2\eta}{c+2\eta-\eta^2}}k_0. \tag{21}$$

Nonpotential models of isotropic patterns generally exhibit nontrivial wave number selection far from onset, with $k < k_c$. The value of k depends on ε and is not determined by any minimization principle [14,22,30,48,49]. We observe similar behavior for the nonpotential anisotropic models. The
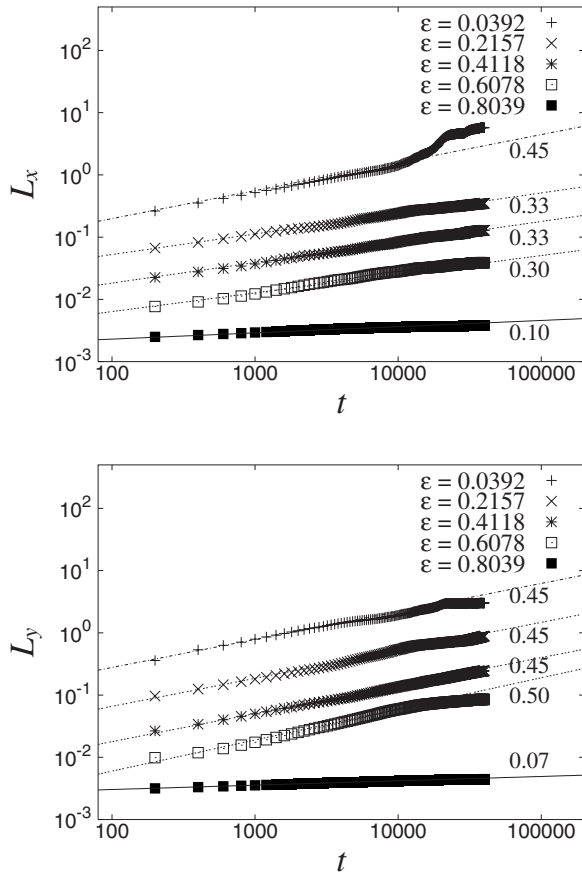
FIG. 3. Correlation lengths along $\hat{x}$ and $\hat{y}$ vs time for model I at different values of ε. The curves have been displaced from their original position for clarity.

FIG. 4. Correlation lengths along $\hat{x}$ and $\hat{y}$ vs time for model II at different values of ε.

selected wave number in the nonpotential models I and II is very close to k_c sufficiently close to onset. As ε is increased, the differences between the three models become more pronounced. For the nonpotential models I and II, k decreases with increasing ε (see Fig. 2), in qualitative agreement with electroconvection experiments far from onset and below the Lifshitz point [40]. This aspect further justifies the use of nonpotential equations for modeling electroconvection. The dependence of k on ε is weaker for model I than for model II, though. In model I, k remains close to the marginal value ($|k-k_c|/k_c<0.03$) even for quench depths as large as $\varepsilon \approx 0.6$.

B. Correlation lengths

The time evolutions of the correlation lengths $L_x(t)$ and $L_y(t)$ are shown in Figs. 3 and 4 for different values of ε and for each nonpotential model.

Close to onset ($\varepsilon=0.0392$), the coarsening rates are well fitted by the power laws

$$L_x(t) \sim t^{1/z_x}, \quad L_y(t) \sim t^{1/z_y}. \tag{22}$$

For both models I and II, we find $1/z_x=1/z_y\approx0.45$ in the intermediate time regime. Finite size effects become important at large times. These results are similar to those obtained for the PK potential model [34], where exponents close to
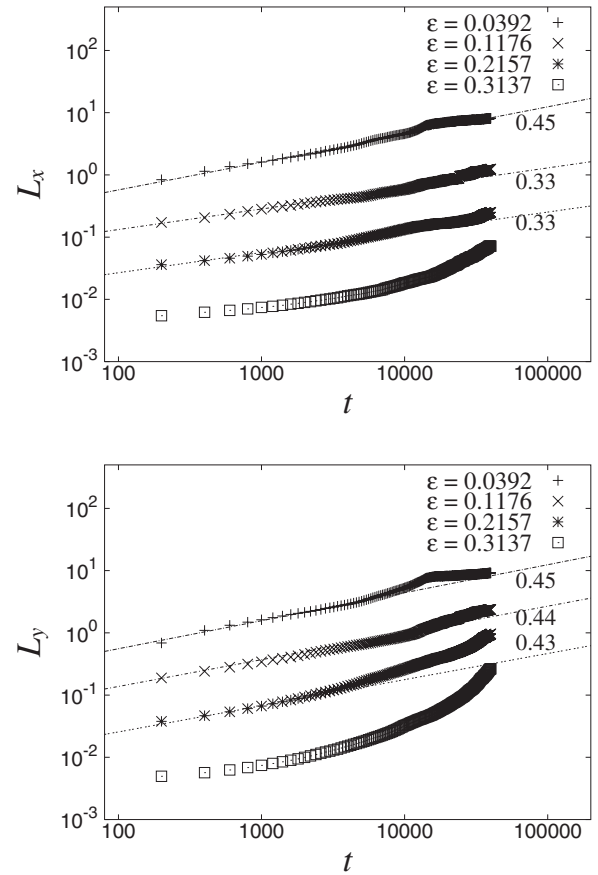
1/2, the value typical of curvature driven growth, were reported near onset. In Sec. V A below, we present analytical arguments showing that the three models proposed can be approximately reduced, close to onset only, to model A for a nonconserved order parameter [3].

At intermediate values of ε, comprised at least in the interval [0.2,0.4] in the case of model I, the growth of both correlation lengths is well fitted by power laws with two distinct exponents $1/z_x\approx0.33$ and $1/z_y\approx0.45$, as shown in Fig. 3. Similar results were obtained for the potential PK model [34]. These features are also observed in model II, but in a smaller interval of values of ε. For $\varepsilon=0.1176$, the scaling laws $L_x\sim t^{0.33}$ and $L_y\sim t^{0.45}$ hold until $t\simeq10^4$; see Fig. 4. This two-exponent regime observed at intermediate quenches in all models indicates that L_y grows faster than L_x. However, as shown in Fig. 5 where both lengths are plotted together for model I, domains are on average longer along $\hat{x}$ than along $\hat{y}$ at short times. Therefore, there is a characteristic time t^* such that $L_x(t^*)=L_y(t^*)$. When $t>t^*$, domains become longer along $\hat{y}$ than along $\hat{x}$. A qualitatively similar behavior is reported in electroconvection experiments in [31], where domains are more elongated along $\hat{x}$ than along $\hat{y}$ at short times, although the growth along $\hat{y}$ is faster.

For deep quenches, the growth rates of $L_x(t)$ and $L_y(t)$ become extremely slow in model I, as shown in Fig. 3 for $\varepsilon=0.8039$. The transition to such arrested dynamics is relatively abrupt, since, for $\varepsilon=0.6078$, L_y and L_y are still well
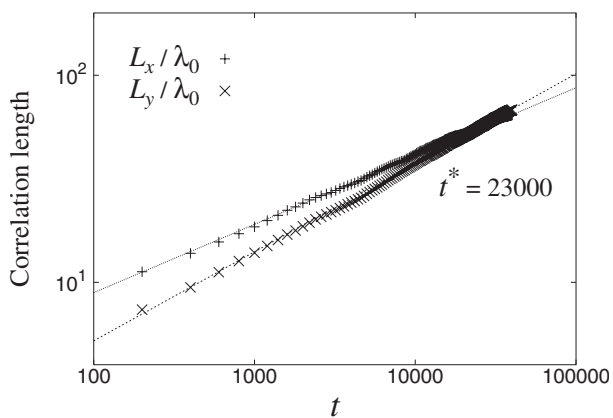
FIG. 5. Time evolution of the correlation lengths along $\hat{x}$ and $\hat{y}$ for model I with $\varepsilon=0.4118$. The characteristic time such that $L_x =L_y$ is $t^* \approx 23\,000$.

described by the laws $t^{1/2}$ and $t^{1/3}$, respectively. Similar frozen states observed in the potential PK model were explained by the presence of pinning effects acting on defects at large quenches [34]. However, as discussed in Sec. V B, freezing probably has a different origin in the nonpotential case.

Whereas the ordering dynamics in model I is similar to that of the potential case for a wide range of values of ε, the nonpotential terms of model II have dramatic effects at large ε. For $\varepsilon=0.2157$ and 0.3137, the correlation lengths grow *faster* than a power law at intermediate and large times; see Fig. 4. Only at short times ($t<10^3$) can an apparent scaling regime with $1/z_x \leq 1/3$ and $1/z_y \leq 0.45$ be observed. A secondary bifurcation from oblique to normal stripes actually occurs in model II close to $\varepsilon \approx 0.4$, preventing the study of oblique domain coarsening for larger quenches.

C. Defect densities

The results presented above are further supported by studying the decay rate of defect densities. Assuming that scaling holds, the total length of chevron boundaries in a system of area A can be estimated as $L_x A/(L_x L_y) \sim 1/L_y$. Similarly, the dislocation density should scale as $1/L_x$. Therefore, one should expect

$$\rho_{dis}(t) \sim L_x(t)^{-1}, \quad \rho_{ch}(t) \sim L_y(t)^{-1} \qquad (23)$$

or

$$\rho_{dis}(t) \sim t^{-1/z_{dis}}, \quad \rho_{ch}(t) \sim t^{-1/z_{ch}}, \qquad (24)$$

with the defect exponents obeying $z_{dis}=z_x$ and $z_{ch}=z_y$.

Figures 6 and 7 show the time evolution of $\rho_{dis}(t)$ and $\rho_{ch}(t)$ for different values of ε in both nonpotential models.

Close to onset ($\varepsilon=0.0392$), the time evolution of dislocation and chevron densities is well fitted by power laws with $1/z_{dis} \approx 1/z_{ch} \approx 0.45$, as shown in Figs. 6 (model I) and 7 (model II). This result further suggests that defect dynamics is isotropic close to onset, in agreement with the arguments exposed below in Sec. V A. Deviations from the laws (24) are observed at late times ($10^4<t$) and are due to finite size effects (see below).
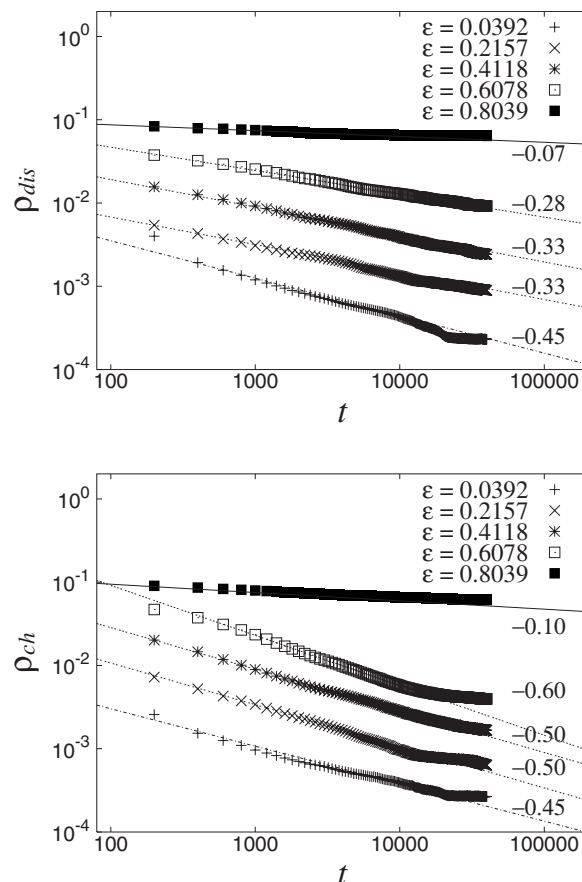

FIG. 6. Dislocation and chevron densities vs time for model I at different values of ε. The curves have been displaced from their original position for clarity.

On increasing ε, the defect dynamics becomes anisotropic and different laws are observed for the two types of defects. Chevron boundaries become quickly pinned and remain practically immobile, whereas coarsening is dominated by dislocation gliding along the horizontal direction. The reduction of the length of a chevron boundary can occur by the motion of the slightly curved dislocation arrays of opposite Burgers vectors located on its sides (see Sec. V). This mechanism was also identified experimentally in electroconvection [32].

In an intermediate range of values of ε, the relations (23) are still satisfied, despite the pinning of the chevron boundaries. As shown in Fig. 6 for model I, for $\varepsilon=0.2157$ and $\varepsilon =0.4118$, $\rho_{dis}(t)$ and $\rho_{ch}(t)$ decay as power laws with two different exponents $z_{dis} \approx 3$ and $z_{ch} \approx 2$. These are the same values as observed in the previous section for z_x and z_y, respectively. Model II leads to the same two exponents for $\varepsilon=0.1176$ and $t<10^4$; see Fig. 7.

Figure 8 shows the evolution of the defect densities obtained from two system sizes 1024×1024 and 512×512, with $\varepsilon=0.2157$. As expected, corrections to scaling occur sooner for the smaller system (at $t \approx 7000$), when the correlation lengths become comparable to the system size.

Note that the $t^{-1/3}$ decay rate for the dislocation density agrees well with the experimental results reported in [32]. However, in this intermediate quench depth regime, our nu-
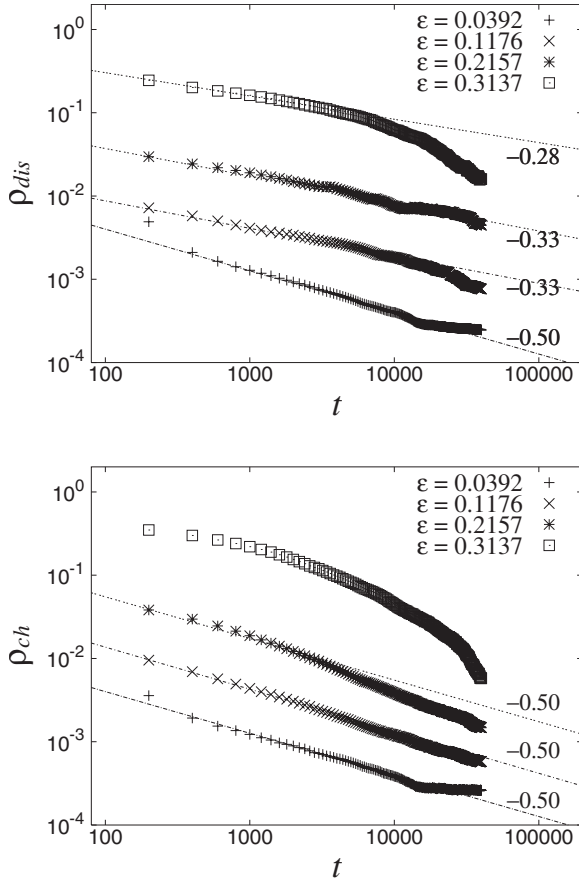
FIG. 7. Dislocation and chevron densities vs time for model II at different values of ε.

merical results predict a much faster decay of the chevron density (as $t^{-1/2}$) than observed experimentally ($t^{-1/5}$ [32]). It is worth noticing that no coarsening laws with exponent 1/2 were ever observed in electroconvection experiments.

At large quenches, dislocation gliding becomes very slow in model I, as shown in Fig. 6 for $\varepsilon = 0.8039$. For $t > 2000$ the defect density saturates to an almost constant value, indicating freezing. As shown below in Sec. V B, the single defect
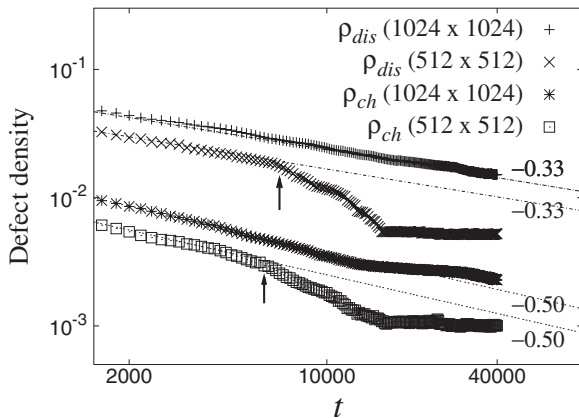

FIG. 8. Late time evolution of the defect densities for model I ($\varepsilon = 0.2157$) for two different lattice sizes (1024×1024 and 512×512 nodes). The arrows indicate the beginning of finite size effects.

dynamics in model I presents some interesting nonrelaxational features at large quenches, which prevent the annihilation of small domains.

In model II, defect annihilation is on the contrary accelerated at large quenches, and densities decay faster than inverse power laws, as shown in Fig. 7 for $\varepsilon = 0.2157$ and 0.3137. These results confirm those of Sec. IV B regarding the correlation lengths. As for the other models, pinning effects might slow down defect motion at short times (up to $t \simeq 1000$), as dislocation and chevron densities decay more slowly than $t^{-1/3}$ and $t^{-1/2}$, respectively. However, nonpotential effects dominate dislocation motion when $t > 1000$ and the oblique stripe pattern quickly reaches fully ordered configurations. In Sec. V B, we show that single defect dynamics is quite different in models I and II far from onset.

Note that coarsening rates faster than a $t^{1/2}$ law for oblique stripes have been reported in electroconvection experiments [50]. These fast coarsening laws were observed when the background wave number is small, a property also shared by model II (see Fig. 2).

D. Dynamical scaling

In the case of the potential model close to onset [34], dynamical scaling properties of the structure factor were investigated along the directions parallel to the wave numbers $\vec{k}_c^+$ and $\vec{k}_c^-$. As shown above, chevron boundaries and dislocations have very different mobilities further from onset. Therefore, it sounds more natural to test one-dimensional scaling relations along $\hat{x}$ and $\hat{y}$ separately. The dynamical scaling hypothesis implies that the structure factors (14) and (15) should obey the ansatz

$$S_x(q_x, t) = L_x(t) f_x(q_x L_x(t)), \tag{25}$$

$$S_y(q_y, t) = L_y(t) f_y(q_y L_y(t)), \tag{26}$$

where $L_x(t)$ and $L_y(t)$ are the characteristic length scales previously defined through relations (18) and (19); f_x and f_y are functions independent of time.

Since the ordering dynamics of the oblique striped domains close to onset can be approximately reduced to the dynamics of model A (see Sec V A), one should expect that dynamical scaling holds along any direction in Fourier space. Figure 9 shows that the ansatz (25) and (26) holds over two time decades for model II close to onset ($\varepsilon = 0.0392$). The same results are observed for the PK potential model and model I (not shown). However, in the region near $k = 0$, the scaling functions in the three models decay rapidly (see Fig. 9) and differ noticeably from that of model A, which is quadratic for small k [51,52]. This unusual behavior may indicate that, given a random initial condition, oblique patterns at early times form different large scale domain structures than in model A.

As ε is increased, isotropic dynamical scaling breaks down because coarsening is characterized by two growing lengths scales with distinct exponents in the $\hat{x}$ and $\hat{y}$ directions. Nevertheless, Fig. 10 (top) shows that the one-dimensional scaling relation (25) in the $\hat{x}$ direction (where $z_x \approx z_{dis} \approx 3$) holds over two time decades for model II. In
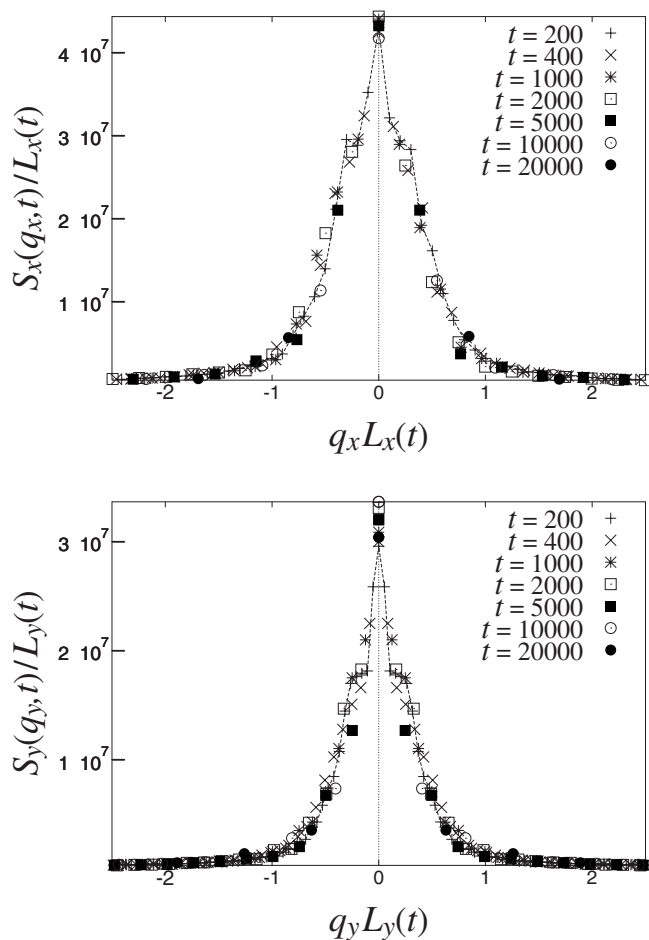
FIG. 9. Dynamical scaling along the $\hat{x}$ and $\hat{y}$ directions for model II close to onset ($\varepsilon = 0.0392$).

FIG. 10. Log-log plot of $S_x(q_x,t)/L_x(t)$ as a function of $q_xL_x(t)$ for model II: $\varepsilon = 0.1176$ (top) and 0.2157 (bottom). Solid lines correspond to Porod's law.

this regime, where $z_y \approx 2$, a similar scaling behavior is also observed along $\hat{y}$ (not shown), for all three models. Deviations from dynamical scaling are observed in the large quench depth regime; see Fig. 10 (bottom).

We verify that the tails of the structure factors obey the well-known Porod's law [2], as illustrated in Fig. 10. If the one-dimensional correlation functions obey a scaling form at short distances, one expects that $S_{x,y}(q_{x,y},t)/L_{x,y}(t) \sim 1/[q_{x,y}L_{x,y}(t)]^{d+1}$ at large $q_{x,y}$, with $d=1$ here.

V. DISCUSSION

A. Mapping to model A in an external field for low-to-moderate quenches

The numerical results obtained *very close to onset* show that the coarsening of oblique stripes is characterized by a single exponent $z_{dis} \approx z_{ch} \approx z_x \approx z_y \approx 2$. This result can be explained by the following weakly nonlinear arguments. The amplitude Eqs. (10) and (11) can be used to describe the dynamics of grain boundaries separating zig and zag domains close to onset ($\varepsilon \ll 1$) in all models. In the absence of grain boundaries, the stationary uniform amplitudes in a zig domain are
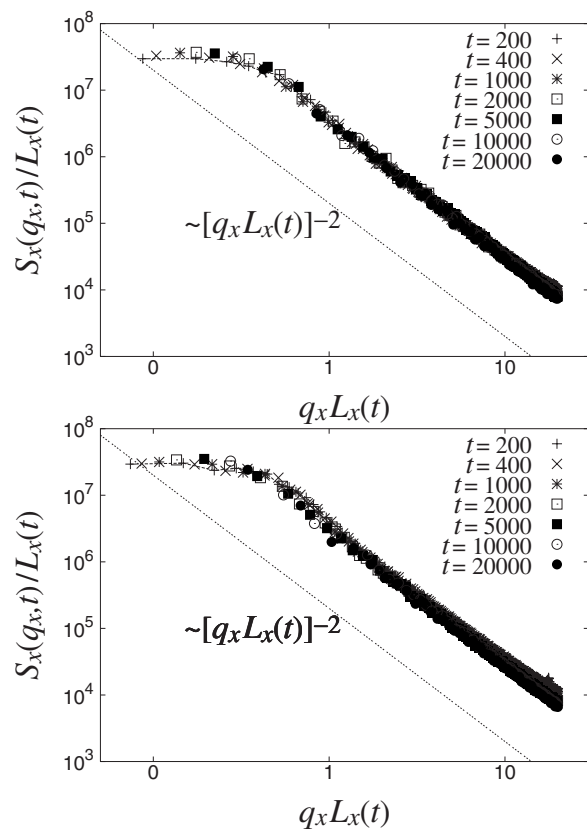
$$a^+ = \sqrt{\frac{\varepsilon}{3\gamma}}, \quad a^- = 0, \tag{27}$$

and vice versa in a zag domain. In the vicinity of a grain boundary, the amplitudes change continuously from one uniform solution to the other along the normal coordinate. Figure 11(a) displays the stationary numerical profiles $a^+(x)$ and $a^-(x)$ of solutions of Eqs. (10) and (11) close to onset for a vertical boundary (dislocation array). The sum $a^+ + a^-$ and difference $a^+ - a^-$ are also plotted in Fig. 11(b). We observe that $a^+ + a^-$ remains close to the constant bulk value $(\varepsilon/3\gamma)^{1/2}$ in the boundary region, while $a^+ - a^-$ changes continuously from $+(\varepsilon/3\gamma)^{1/2}$ (zig domain) to $-(\varepsilon/3\gamma)^{1/2}$ (zag domain). For any polycrystalline configuration, we define the local order parameters $\phi^+ \equiv A^+ + A^-$ and $\phi^- \equiv A^+ - A^- \equiv \sqrt{\varepsilon/3\gamma}\psi_d$, which redefines the orientational order parameter field ψ_d. Based on Fig. 11(b), we approximate ϕ^+ to a constant, even in configurations containing many interfaces:

$$\phi^+(\vec{r},t) \simeq \sqrt{\frac{\varepsilon}{3\gamma}}. \tag{28}$$

To find an equation for the local orientational order parameter ψ_d, we substitute the new fields into (10) and (11). By making the change of variables
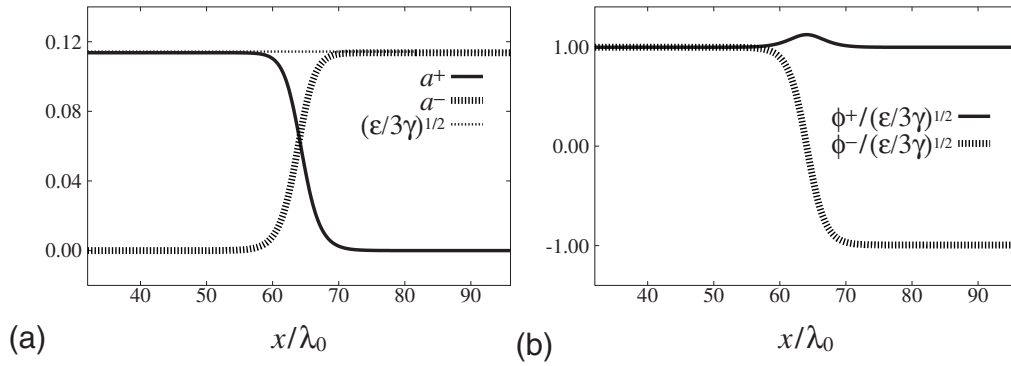
FIG. 11. (a) Stationary numerical solutions $(a^+(x), a^-(x))$ of Eqs. (10) and (11) for a vertical planar grain boundary, with $\varepsilon = 0.0392$, $c = 12$, $\eta = 0.5$, and $\gamma = 1$; (b) $\phi^+ = a^+ + a^-$ and $\phi^- = a^+ - a^-$ as functions of x.

$$X = \left(\frac{c + 2\eta - \eta^2}{c + \eta} \varepsilon \right)^{1/2} x, \quad Y = \left(\frac{c + 2\eta - \eta^2}{(1+c)\eta} \varepsilon \right)^{1/2} y,$$
(29)

we obtain

$$\partial_T \psi_d = \frac{3}{4} \psi_d + \frac{4}{k_0^2} \nabla^2 \psi_d - \frac{3}{4} \psi_d^3,$$
(30)

where $T = \varepsilon t$ and $\nabla^2 = \partial_X^2 + \partial_Y^2$. This isotropic equation is easily recast into the well-known model A for a nonconserved order parameter [2,3,7]: $\partial_t \psi_d = \psi_d + \nabla^2 \psi_d - \psi_d^3$. Hence, as previously suggested [34], the coarsening of oblique stripes close to onset is isotropic [after the coordinate change (29)] and driven by curvature, with a length scale increasing as $t^{1/2}$. Such a regime has never been observed experimentally in electroconvection, despite the fact that the amplitude Eqs. (10) and (11) should *a priori* describe this system correctly close enough to onset [43–45].

Further from onset, at intermediate values of ε, the horizontal (chevron) grain boundaries become pinned in the three models considered. In pattern forming systems, defect pinning often arises from the coupling between the amplitudes varying slowly in space and the short period modulations of the local order parameter [19,42,53]. This coupling generates "nonadiabatic" terms in the amplitude equations, which oscillate with the spatial coordinates and create periodic energy barriers for defects. The simplest generalization of model A that incorporates similar pinning effects for horizontal interfaces is

$$\partial_t \psi_d = \psi_d + \nabla^2 \psi_d - \psi_d^3 + p \cos(k_p y),$$
(31)

where the periodicity of the pinning potential, of magnitude p, is *smaller* than the interface width ($2\pi/k_p < 1$). The above equation describes the ordering kinetics of a nonconserved scalar order parameter in a stationary, spatially modulated external field.

As discussed in [34], chevron boundaries pin at intermediate values of ε while dislocations are still mobile. This effect can be explained by the fact that the magnitude of the pinning potential of chevrons (p) is orders of magnitude higher than that of dislocation arrays. A detailed calculation showing this and further supporting the reduced model (31)

will be presented elsewhere. Model A is recovered close to onset because pinning potentials tend to zero very rapidly as $\varepsilon \to 0$, independently of the interface orientation [19,42]. Equation (31) can also be modified by replacing p by a term proportional to $(\psi_d)^2 \partial_y \psi_d$, so that the external field acts mostly on horizontal boundaries and not in the bulk.

B. Nonrelaxational defect dynamics far from onset

Some qualitative insights into domain coarsening for models I and II far from onset can be gained by numerically studying the shrinking dynamics of an initially rectangular zag domain embedded in a zig surrounding. The background wave number is initially fixed to the value k_c.

Figure 12(a) shows the results obtained by solving model I with an embedded domain of vertical width $D_y = 20\lambda_c$ and $\varepsilon = 0.2157$. At this moderate quench, the dynamics is approximately driven by the decrease of the energy (12) through the reduction of total interface length. As mentioned in the previous sections, chevron boundaries are pinned and the reduction of their length is achieved by the motion of the curved lateral dislocation arrays. When colliding, dislocations of opposite Burgers vectors annihilate, as also observed experimentally [32].

Figure 12(b) shows the evolution of the same initial domain further from onset ($\varepsilon = 0.6078$). In this case dislocation motion is not restricted to reducing the chevron length. The boundaries exhibit a more complex dynamics instead and the domain shape breaks its initial axial symmetry.

To study the transition between these two dynamical regimes for model I, we report in the upper panel of Fig. 13 the evolution of the area $A_d(t)$ of an embedded domain. At moderate values of ε, $A_d(t)$ continuously decreases in time at a rather constant rate as the zag domain shrinks. However, above a critical value, $\varepsilon_c \approx 0.6$ for a domain of width $D_y = 32\lambda_c$, $A_d(t)$ tends toward a *finite* value at large times, suggesting that dislocations effectively repel each other. The transition between the two regimes is fairly abrupt. This situation is reminiscent of dislocation motion modes observed experimentally, where walls of oppositely charged defects can approach within some distance and then move apart [32]. The results above provide a picture of the arrested growth of order observed far from onset in model I. The same single-
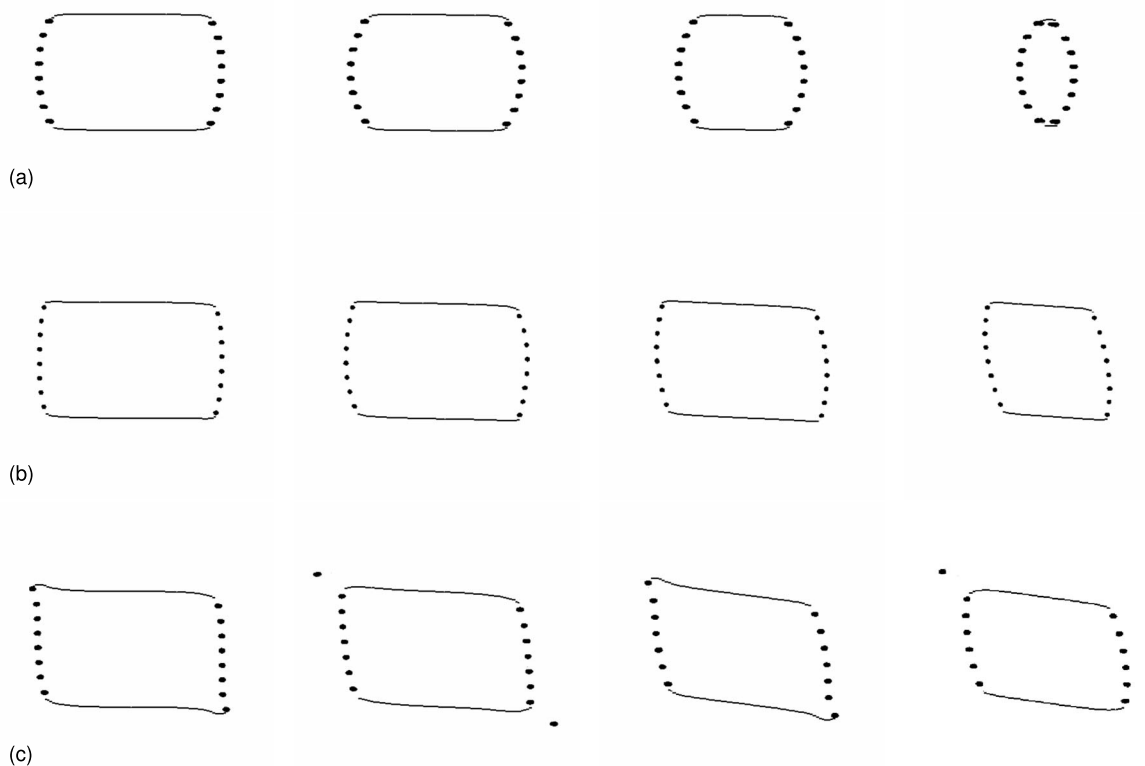
FIG. 12. Defect field of an initially rectangular zag domain surrounded by zig stripes, for model I with (a) $\varepsilon = 0.2157$ at $t = 200$, 600, 1800, and 3600, and (b) $\varepsilon = 0.6078$ at $t = 200$, 600, 1800, and 12000; and (c) for model II with $\varepsilon = 0.2157$ at $t = 200$, 600, 1800, and 2400.

domain calculation using the PK potential model with $\varepsilon = 0.6078$, a value close to the above ε_c, shows that the domain completely shrinks (the bullet symbols of Fig. 13).

We therefore conclude that, unlike in potential models, the arrested ordering kinetics in model I is primarily due to nonpotential repulsion effects among dislocations, and not to dislocation pinning induced by nonadiabatic effects (although these might also be present).

The lower panel of Fig. 13 shows that, for model I, the critical value ε_c defined above depends on the domain vertical width. Interestingly, ε_c seems to tend toward a constant value (~ 0.5) as $D_y \rightarrow \infty$, meaning that below this parameter value all domains shrink (coarsening regime). For $\varepsilon > 0.5$, large enough domains do not shrink (disordered regime). This diagram suggests that model I undergoes a transition to arrested coarsening as ε crosses a critical value.

Figure 12(c) shows the evolution of a shrinking domain in model II, for $\varepsilon = 0.2157$. An effective dislocation repulsion is also observed, leading, in contrast to model I, to the emission of pairs of oppositely charged dislocations. This mechanism gradually reduces the average domain width. For this value of ε, the ordering kinetics of polycrystalline configurations is faster than a power law. Dislocation emission by shrinking domains at large quenches could be responsible for the very fast coarsening laws observed in model II.

VI. SUMMARY AND CONCLUDING REMARKS

We have studied the coarsening of two-dimensional oblique stripe phases by using two nonpotential Swift-Hohenberg-like equations. The results have been compared to previous ones obtained in the potential case [34].

Close to onset ($\varepsilon \ll 1$), the patterns can be described in all cases by two coupled amplitude equations that can be reduced approximately to model A for a nonconserved scalar order parameter. Consequently, the coarsening process close to onset is self-similar, and domain growth is characterized by a single length scale growing as $t^{1/z}$ with $z \approx 2$.

At intermediate values of ε, a second regime is observed in both potential and nonpotential models, where chevron boundaries become pinned, and domain growth is driven by the horizontal motion of curved dislocation arrays. The one-dimensional correlation functions along the $\hat{x}$ and $\hat{y}$ directions still obey dynamical scaling relations, but the corresponding correlation lengths grow at different rates: $L_x(t) \sim t^{1/z_x}$ and $L_y(t) \sim t^{1/z_y}$, with $z_x \approx 3$ and $z_y \approx 2$. In this regime, the system should be well described by a model A equation in an external modulated field [Eq. (31)].

The nonpotential equations studied here reproduce qualitatively the observed selected wave numbers in electroconvection experiments [40]. The unusual but apparently robust $t^{1/3}$ law for L_x also agrees with experimental data [32]. How-
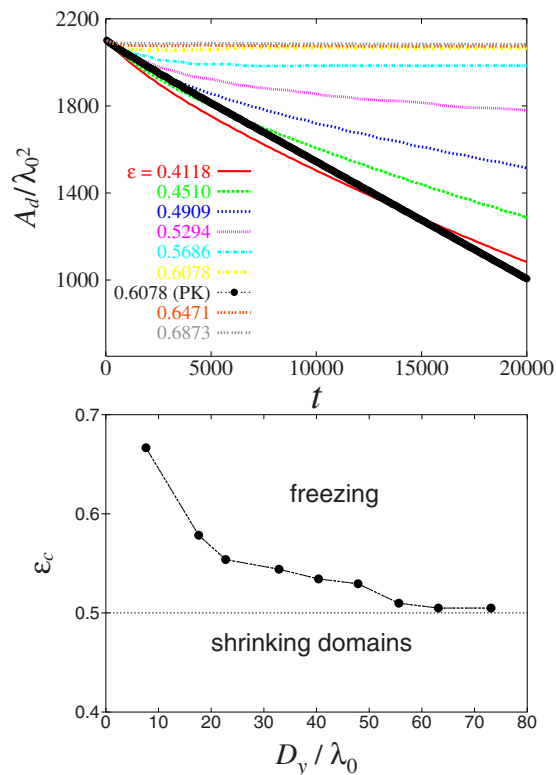
FIG. 13. (Color online) Upper panel: Time evolution of the area of an initially rectangular zag domain of fixed width $D_y = 32\lambda_c$ surrounded by zig stripes, for model I and different values of ε (increasing from bottom to top). Lower panel: Critical parameter value above which a domain does not shrink, as a function of the domain width. Below the dotted line, all domains were observed to shrink.

ever, no 1/2 exponents were ever observed experimentally.

When $\varepsilon \sim O(1)$, a third regime can be identified, where the defect dynamics differs noticeably in potential and nonpotential models. In the potential and nonpotential I cases, coarsening rates become very slow at late times, the system remaining in macroscopically disordered states. Whereas freezing is due to dislocation pinning in the potential case [34], in model I nonrelaxational effects dominate, leading to a complex dislocation dynamics (quite similar to the experimental observations of Ref. [32]) that prevents small domains from shrinking. The study of the relaxation of single domains suggest that this transition to arrested coarsening in model I is abrupt. This result is surprising, as it is generally accepted that nonpotential effects enhance coarsening [14,25,54]. For model II, nonpotential effects also affect dislocation dynamics but lead to the opposite macroscopic behavior: defect densities decay in time faster than a power law and the system orders very quickly.

A better understanding of the transitions between the different coarsening regimes far from onset requires a systematic study of the dynamics of shrinking domains and its role in wave number selection. In this spirit, a study of grain boundary motion in nonpotential stripe patterns was recently performed for isotropic systems [30]. We hope that the study of defect motion in nonpotential systems far from onset will motivate new experiments.

Finally, recent experiments [33] studying the impact of noise on the coarsening rates of oblique rolls could also motivate future research.

[1] J. D. Gunton, M. San Miguel, and P. S. Sahni, *Phase Transitions and Critical Phenomena* (Academic, New York, 1989).

[2] A. Bray, Adv. Phys. **43**, 357 (1994).

[3] P. Hohenberg and P. Halperin, Rev. Mod. Phys. **49**, 435 (1977).

[4] A. J. Bray and A. D. Rutenberg, Phys. Rev. E **49**, R27 (1994).

[5] A. J. Bray, Phys. Rev. E **58**, 1508 (1998).

[6] I. M. Lifshitz and V. V. Slyozov, J. Phys. Chem. Solids **19**, 35 (1961).

[7] S. M. Allen and J. W. Cahn, Acta Metall. **27**, 1085 (1979).

[8] M. C. Cross and P. C. Hohenberg, Rev. Mod. Phys. **65**, 851 (1993).

[9] C. Bowman and A. C. Newell, Rev. Mod. Phys. **70**, 289 (1998).

[10] J. P. Gollub and J. S. Langer, Rev. Mod. Phys. **71**, S396 (1999).

[11] M. I. Rabinovich, A. B. Ezersky, and P. D. Weidman, *The Dynamics of Patterns* (World Scientific, Singapore, 2000).

[12] K. R. Elder, J. Vinals, and M. Grant, Phys. Rev. Lett. **68**, 3024 (1992).

[13] K. R. Elder, J. Vinals, and M. Grant, Phys. Rev. A **46**, 7618 (1992).

[14] M. C. Cross and D. I. Meiron, Phys. Rev. Lett. **75**, 2152 (1995).

[15] Q. Hou, S. Sasa, and N. Goldenfeld, Physica A **239**, 219 (1997).

[16] J. J. Christensen and A. J. Bray, Phys. Rev. E **58**, 5364 (1998).

[17] D. Boyer and J. Vinals, Phys. Rev. E **64**, 050101(R) (2001).

[18] T. Taneike, T. Nihei, and Y. Shiwa, Phys. Lett. A **303**, 212 (2002).

[19] D. Boyer and J. Vinals, Phys. Rev. E **65**, 046119 (2002).

[20] H. Qian and G. F. Mazenko, Phys. Rev. E **67**, 036102 (2003).

[21] H. Qian and G. F. Mazenko, Phys. Rev. E **68**, 021109 (2003).

[22] M. R. Paul, K.-H. Chiam, M. C. Cross, and P. F. Fischer, Phys. Rev. Lett. **93**, 064503 (2004).

[23] T. Galla and E. Moro, Phys. Rev. E **67**, 035101(R) (2003).

[24] A. Xu, G. Gonnella, A. Lamura, G. Amati, and F. Massaioli, Europhys. Lett. **71**, 651 (2005).

[25] Y. Yokojima and Y. Shiwa, Phys. Rev. E **65**, 056308 (2002).

[26] C. Harrison *et al.*, Science **290**, 1558 (2000).

[27] C. Harrison, Z. Cheng, S. Sethuraman, D. A. Huse, P. M. Chaikin, D. A. Vega, J. M. Sebastian, R. A. Register, and D. H.

Adamson, Phys. Rev. E **66**, 011706 (2002).

[28] R. Ruiz, R. L. Sandstrom, and C. T. Black, Adv. Mater. (Weinheim, Ger.) **19**, 587 (2007).

[29] P. Manneville, *Dissipative Structures and Weak Turbulence* (Academic, New York, 1990).

[30] Z.F. Huang and J. Vinals, Phys. Rev. E **75**, 056202 (2007).

[31] L. Purvis and M. Dennin, Phys. Rev. Lett. **86**, 5898 (2001).

[32] C. Kamaga, F. Ibrahim, and M. Dennin, Phys. Rev. E **69**, 066213 (2004).

[33] M. Griffith and M. Dennin, Phys. Rev. E **74**, 027201 (2006).

[34] D. Boyer, Phys. Rev. E **69**, 066111 (2004).

[35] H. Q. Qian and G. F. Mazenko, Phys. Rev. E **73**, 036117 (2006).

[36] W. Pesch and L. Kramer, Z. Phys. B: Condens. Matter **63**, 121 (1986).

[37] L. Kramer and W. Pesch, Annu. Rev. Fluid Mech. **27**, 515 (1995).

[38] A. Buka and L. Kramer, *Pattern Formation in Liquid Crystals* (Springer-Verlag, New York, 1996).

[39] M. Dennin, D. S. Cannell, and G. Ahlers, Phys. Rev. E **57**, 638 (1998).

[40] D. Funfschilling, B. Sammuli, and M. Dennin, Phys. Rev. E **67**, 016207 (2003).

[41] H. S. Greenside and M. C. Cross, Phys. Rev. A **31**, 2492 (1985).

[42] B. A. Malomed, A. A. Nepomnyashchy, and M. I. Tribelsky, Phys. Rev. A **42**, 7244 (1990).

[43] E. Bodenschatz, W. Pesch, and L. Kramer, Physica D. **32**, 135 (1988).

[44] M. Treiber and L. Kramer, Phys. Rev. E **58**, 1973 (1998).

[45] E. Plaut and R. Ribotta, Eur. Phys. J. B **5**, 265 (1998).

[46] M. C. Cross, D. Meiron, and Y. Tu, Chaos **4**, 607 (1994).

[47] D. R. Nelson, *Defects and Geometry in Condensed Matter Physics* (Cambridge University Press, Cambridge, U.K., 2002).

[48] A. Hari and A. A. Nepomnyashchy, Phys. Rev. E **61**, 4835 (2000).

[49] G. Tesauro and M. C. Cross, Phys. Rev. A **34**, 1363 (1986).

[50] C. Kamaga, D. Funfschilling, and M. Dennin, Phys. Rev. E **69**, 016308 (2004).

[51] T. Ohta, D. Jasnow, and K. Kawasaki, Phys. Rev. Lett. **49**, 1223 (1982).

[52] S. Puri and Y. Oono, Phys. Rev. A **38**, 1542 (1988).

[53] Y. Pomeau, Physica D **23**, 3 (1986).

[54] R. Gallego, M. S. Miguel, and R. Toral, Phys. Rev. E **58**, 3125 (1998).